We are IntechOpen, the world's leading publisher of Open Access books Built by scientists, for scientists

5,300
Open access books available

130,000
International authors and editors

155M
Downloads

Our authors are among the

154
Countries delivered to

TOP 1%
most cited scientists

12.2%
Contributors from top 500 universities

CLARIVATE ANALYTICS BOOK CITATION INDEX INDEXED

WEB OF SCIENCE™

Selection of our books indexed in the Book Citation Index in Web of Science™ Core Collection (BKCI)

Interested in publishing with us?
Contact book.department@intechopen.com

Numbers displayed above are based on latest data collected.
For more information visit www.intechopen.com

Chapter

Fourier Transform Infrared Spectroscopy of the Animal Tissues

Vineet Kumar, Shruti D. Vora, Foram A. Asodiya, Naveen Kumar and Anil K. Gangwar

Abstract

Animal tissues are extensively used as scaffolds for tissue engineering and regenerative therapies. They are typically subjected to decellularization process to obtain a cell-free extracellular matrix (ECM) scaffolds. It is important to identify chemical structure of the ECM scaffolds and Fourier transform infrared (FTIR) appears to be a technique of choice. In this chapter, FTIR spectra of native and decellularized buffalo aortae, buffalo diaphragms, goat skin, and native bovine cortical bone are presented. The transmittance peaks are that of organic collagen amide A, amide B, amide I, amide II and amide III chemical functional groups in both native and decellularized aortae, diaphragms and skin. In bone, the transmittance peaks are that of inorganic ν_1, ν_3 PO_4^{3-}, OH^- in addition to organic collagen amide A, amide B, amide I, amide II and amide III chemical functional groups. These important transmittance peaks of the tissue samples will help researchers in defining the chemical structure of these animal tissues.

Keywords: buffalo aorta, buffalo diaphragm, bovine bone, goat skin, Fourier transform infrared spectroscopy

1. Introduction

The extracellular matrix (ECM) scaffolds primarily composed of structural collagen protein are widely used in tissue engineering and regenerative medicine [1–15]. These are usually prepared from animal tissues by decellularization process. Decellularization is the process of removal of native cells from animal tissue, leaving behind a three-dimensional network of ECM proteins while preserving the bioactivity and mechanics of the tissue. In the decellularization process, animal tissues are subjected to physical, enzymatic and chemical treatments. Physical methods of decellularization include freezing, direct pressure, sonication, and agitation [16]. Enzymatic techniques of decellularization include the use of protease (trypsin) [1–5, 8, 10, 12–15], endonucleases and exonucleases. Chemical methods of decellularization include the use of acids and alkalis (acetic acid, peracetic acid, hydrochloric acid, sulfuric acid, ammonium hydroxide), nonionic detergents (Triton X-100), ionic detergents (sodium dodecyl sulfate, sodium deoxycholate, Triton X-200) [1–15], zwitterionic detergents (3-[(3-cholamidopropyl)dimethylammonio]-1-propanesulfonate, sulfobetaine-10, sulfobetaine-16), organic solvent (Tri(n-butyl)phosphate) [3, 10], hypertonic and

hypotonic solutions [2, 3, 8, 10, 13, 15], and chelating agents (EDTA). These reagents at higher concentrations extensively disrupt the structural proteins of ECM scaffolds and make it impossible to analyze by routine techniques [17]. Fourier transform infrared (FTIR) spectroscopy is one of the preferred technique for identification of biomolecules through the study of their characteristic vibrational movements [11, 13, 14, 18]. This technique is simple, reproducible, nondestructive to the tissue, and only small amounts of tissue (micrograms to nanograms) with a minimum preparation are required. In addition, this technique also provides molecular-level information allowing investigation of functional groups, bonding types, and molecular conformations. The characteristic peaks in FTIR spectra are molecule specific and provide direct information about biochemical composition. This chapter highlights the application of FTIR spectroscopy for characterization of native and decellularized buffalo aortae, buffalo diaphragms, goat skin, and native bovine cortical bone.

2. Materials

2.1 Chemicals and reagents

Sodium dodecyl sulfate (SDS), Trypsin, Sodium chloride (NaCl), Phosphate-buffered saline (PBS), Ethylene diaminetetraacetic acid (EDTA), Sodium azide (NaN_3), Gentamicin, Potassium bromide (KBr) powder. All the chemicals and reagents used were of the high purity and obtained from Sigma-Aldrich (St. Louis, MO, USA) unless mentioned otherwise. All solutions were prepared fresh using deionized water and analytical grade chemicals at room temperature (unless indicated otherwise).

2.2 Equipments

Magnetic stirrer (C-MAG HS7, IKA, USA), Analytical digital lab balance (Citizen Enterprises, Delhi, India), Fourier transform infrared spectrophotometer (FTIR 8400 s Shimadzu Corporation, Tokyo, Japan), Bard Parker blade number 24, Autoclaved sterile dissecting scissors, Autoclaved sterile jar (Borosil, India), Sterile measuring cylinders (Borosil, India), Dishes (Borosil, India) and Protective equipment such as surgical gloves and surgical autoclaved instruments were used.

2.3 Tissue samples

Fresh cadaver buffalo aorta (**Figure 1A**), buffalo diaphragm (**Figure 1B**) and goat skin (**Figure 1C**) collected in chilled (4°C) sterile 1X PBS (pH 7.4) containing 0.016% gentamicin (antibiotic), 0.0205% EDTA (proteolytic inhibitor) and 0.1% NaN_3 (antimycotic) were our study materials. A cortical bone collected from the anterior diaphysis of the right femur of an adult cadaver Gir cow was also used.

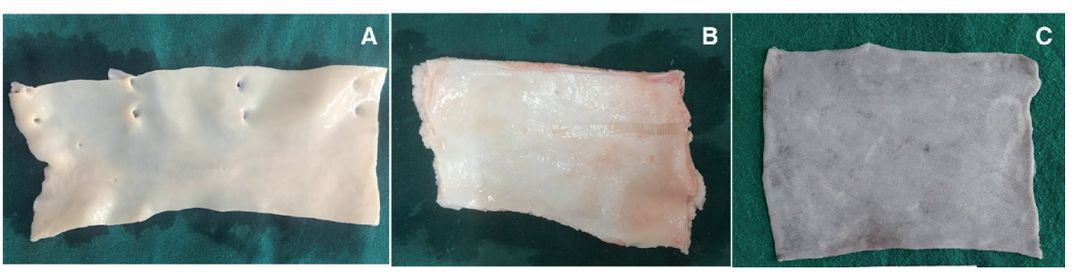

Figure 1.
Gross images of buffalo aorta (a), buffalo diaphragm (B), and goat skin (C).

3. Methods

3.1 Fourier transform infrared spectroscopy of the buffalo aorta

The *aorta,* an elastic artery, has a trilaminar structure consisting of a tunica intima, media, and adventitia. The media comprises cellular elements (including smooth muscle cells) and structural proteins (notably collagen and elastin) that form the ECM. Before being used in regenerative therapies, cellular elements of the aorta should be removed by decellularization process. The decellularization of fresh posterior aorta from deceased donor buffalo was completely achieved by treatment with 1% SDS for 24 hours followed by 0.25% trypsin for 2 hours and again by 1% SDS for 24 hours [19]. Both the native and decellularized aortae were characterized by FTIR spectroscopy [14]. Herein, one milligram of each freeze-dried tissues were mixed with pure dry KBr powder in 1:10 ratio, and pelleted. The FTIR spectra were recorded by an infrared spectrophotometer in the 500–4000 cm^{-1} wave number spectral range with a spectral resolution of 2 cm^{-1} and 45 scans. **Figure 2** illustrates the FTIR spectra of native and decellularized aortae. The transmittance peaks indicated the presence of organic collagen amide A, amide B, amide I, amide II and amide III chemical functional groups in both native and decellularized aortae. The amide A band (3294 cm^{-1}) is associated with H-bonded N-H stretching [11, 13, 20] and was found at 3282.95 cm^{-1} for native aorta and 3280 cm^{-1} for decellularized aorta. The amide B band (2953 and 2928 cm^{-1}) is related to CH_2 asymmetric stretching [11, 13, 21] and was observed at 2958.9 cm^{-1} for native aorta and 2954.08 cm^{-1} for decellularized aorta. The amide I band (1641–1658 cm^{-1}) is associated with C=O hydrogen bonded stretching [11, 13, 22] as recorded at 1658.84 cm^{-1} for native aorta and 1658.84 cm^{-1} for decellularized aorta. The amide II (1539–1546 cm^{-1}) is associated with C-N stretching and N-H in plane bending from amide linkages, including wagging vibrations of CH_2 groups from the glycine backbone and proline side-chains [11, 13, 23] in native aorta and decellularized aorta appeared at 1526.71 cm^{-1} and 1529.60 cm^{-1}, respectively. The amide III (NH bend) band was found at 1282.55 cm^{-1} for NA and 1230.69 cm^{-1} for decellularized aorta [11, 13, 24].

3.2 Fourier transform infrared spectroscopy of the buffalo diaphragm

The diaphragm is a dome shaped structure, composed of muscle surrounding a central tendon, which separates the thoracic and abdominal cavities. Before

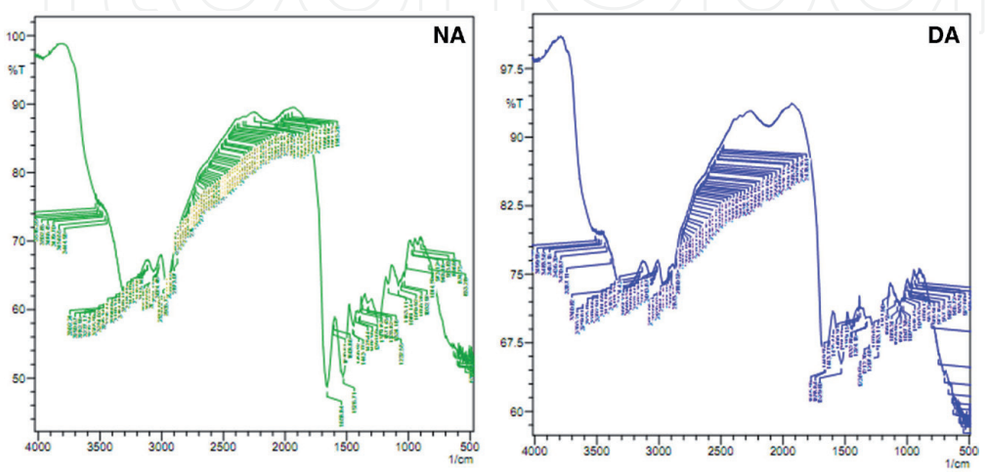

Figure 2.
FTIR spectra showing transmittance peaks of native aorta (NA) at 1282.55, 1526.71, 1658.84, 2958.9 and 3282.95 cm^{-1}; and decellularized aorta (DA) at 1230.69, 1529.60, 1658.84, 2954.08 and 3280 cm^{-1}.

the clinical application, fresh tendinous portion of diaphragm from deceased donor buffalo was decellularized using 2% SDS solution for 48 hours and FTIR spectroscopic characterization was performed [11]. Herein, one milligram of each freeze-dried native and decellularized diaphragms were mixed with pure dry KBr powder in 1:10 ratio, and pelleted. The FTIR spectra were recorded by an infrared spectrophotometer in the 500–4000 cm^{-1} wave number spectral range with a spectral resolution of 2 cm^{-1} and 45 scans. The FTIR spectra of native and decellularized diaphragms are illustrated in the **Figure 3**. The transmittance peaks indicated the presence of organic collagen amide A, amide B, amide I, amide II and amide III chemical functional groups in both native and decellularized diaphragms. The amide A band is associated with H-bonded N-H stretching [20] and was found at 3386.15 cm^{-1} for native diaphragm and 3343.71 cm^{-1} for decellularized diaphragm. The amide B band is related to CH_2 asymmetric stretching [21] and was observed at 2955.04 cm^{-1} for native diaphragm and 2954.08 cm^{-1} for decellularized diaphragm. The amide I band is associated with C=O hydrogen bonded stretching [22] as recorded at 1657.87 cm^{-1} for native diaphragm and 1649.19 cm^{-1} for decellularized diaphragm. The amide II is associated with C-N stretching and N-H in plane bending from amide linkages, including wagging vibrations of CH_2 groups from the glycine backbone and proline side-chains [23] in native diaphragm and decellularized diaphragm appeared at 1535.39 cm^{-1} and 1534.11 cm^{-1}, respectively. The amide III band was found at 1238.34 cm^{-1} for native diaphragm and 1220.02 cm^{-1} for decellularized diaphragm confirming presence of hydrogen bonds [24].

3.3 Fourier transform infrared spectroscopy of the goat skin

The goat skin consists of two layers; superficial epidermis, composed of stratified squamous keratinized epithelium and underlying dermis, composed of dense, irregular connective tissue mainly collagen fibers. Skin appendages such as hair follicles, sebaceous and sweat glands were found in the dermis. The deepithelialization of fresh goat skin was completely achieved by treatment with 0.25% trypsin in 4 mol/L NaCl for 8 hours. Further treatment with 2% SDS for 48 hours demonstrated complete decellularization of the cellular dermis [13]. Native, deepithelialized and decellularized goat skins were characterized by FTIR spectroscopy [13]. One milligram of each freeze-dried native, deepithelialized and decellularized skins were mixed with pure dry KBr powder in 1: 10 ratio, and pelleted. The FTIR spectra were recorded by an infrared spectrophotometer in the 500–4000 cm^{-1}

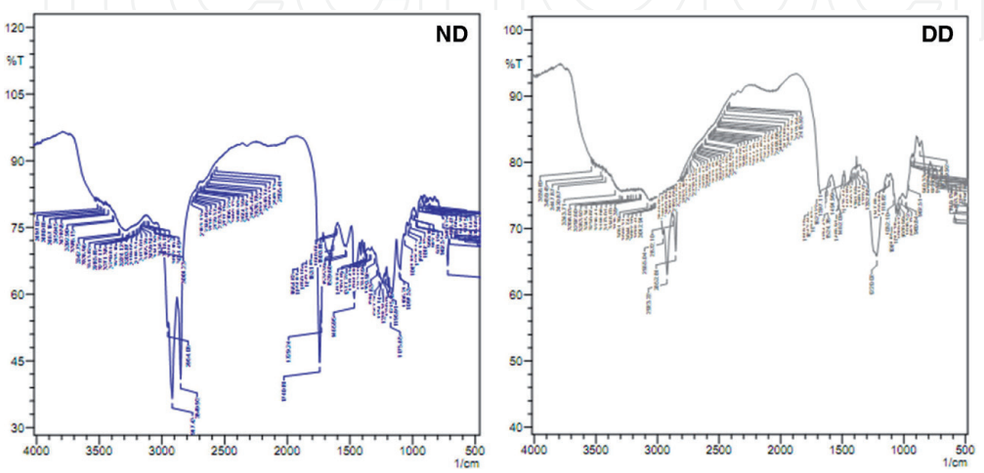

Figure 3.
FTIR spectra showing transmittance peaks of the native diaphragm (ND) at 1238.34, 1535.39, 1657.87, 2955.04 and 3386.15 cm^{-1}; decellularized diaphragm (DD) at 1220.02, 1534.11, 1649.19, 2954.08 and 3343.71 cm^{-1}.

wave-number spectral range with a spectral resolution of 2 cm^{-1} and 45 scans. The FTIR spectra of native, deepithelialized and decellularized skins are illustrated in the **Figure 4**. The transmittance peaks indicated the presence of organic collagen amide A, amide B, amide I, amide II and amide III chemical functional groups in native, deepithelialized and decellularized skins. The peaks at 3288.74 cm^{-1} for native skin, 3289.70 cm^{-1} for deepithelialized skin and 3306.10 cm^{-1} for decellularized skin corresponds to the amide A band (3294 cm^{-1}) of collagen is due to N-H stretching vibrations when the N-H group of the peptide is involved in hydrogen bonds [20]. The peaks at 2936.72 cm^{-1} for native skin, 2953.12 cm^{-1} for deepithelialized skin and 2953.12 cm^{-1} for decellularized skin corresponds to the amide B band (2953 and 2928 cm^{-1}) is due to asymmetric stretching of the CH_2 stretching vibration [21]. The peaks at 1657.87 cm^{-1} for native skin, 1658.84 cm^{-1} for deepithelialized skin and 1666.55 cm^{-1} for decellularized skin corresponds to the amide I band (1641–1658 cm^{-1}) is due to the stretching vibration of the peptide carbonyl group (-C=O) along the polypeptide backbone [22]. The peaks at 1546.96 cm^{-1} for native skin, 1530.57 cm^{-1} for deepithelialized skin and 1547.93 cm^{-1} decellularized skin corresponds to the amide II (1500–1560 cm^{-1}) which arises from the N-H bending vibration coupled to C-N stretching [23]. Amide III band was found at 1236.41 cm^{-1} for NCS, 1238.34 cm^{-1} for DCS, 1238.34 cm^{-1} for CADM, and 1238.34 cm^{-1} for BSC confirming the presence of hydrogen bonds [24].

3.4 Fourier transform infrared spectroscopy of the bovine bone

Bone is a composite biomaterial mainly composed of organic collagen fibers (chiefly type I collagen) and inorganic hydroxyapatite [$Ca_{10}(PO)_6(OH)_2$] crystals. Both the components of bone have specific chemical signatures and, consequently, distinctive infrared spectra at the molecular level [18]. The FTIR spectroscopy of the bovine bone tissue was described in a recent study in which one milligram of powdered native cortical bone was mixed with pure dry KBr powder in 1:10 ratio, and pelleted. The FTIR spectrum was recorded by an infrared spectrophotometer

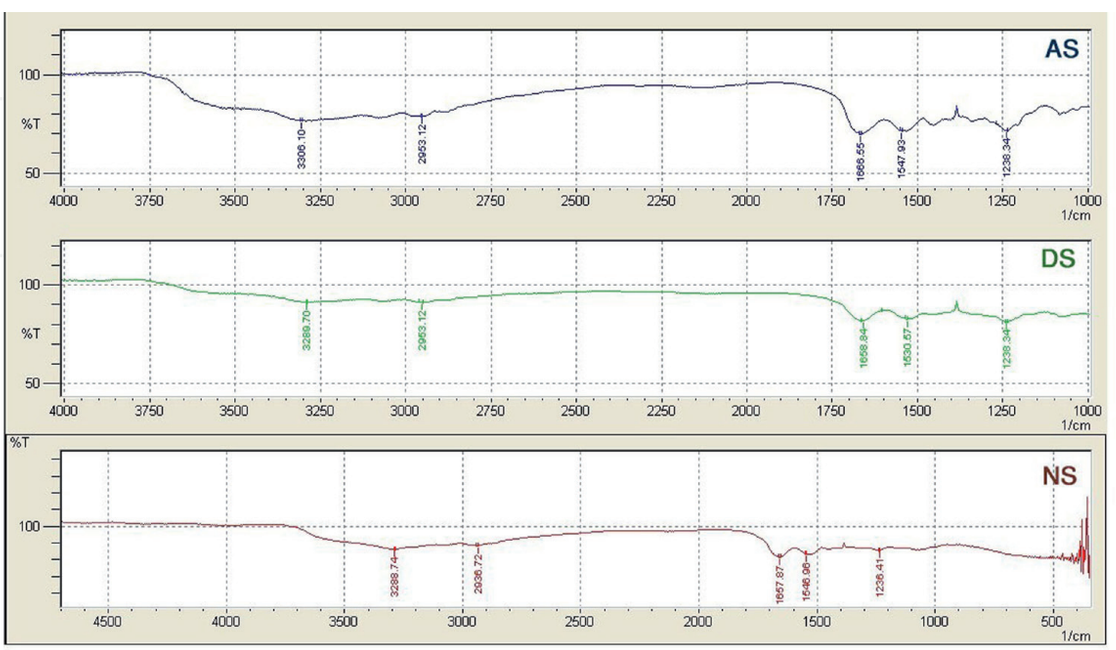

Figure 4.
FTIR spectra showing peaks of native goat skin (NS) at 1236.41, 1546.96, 1657.87, 2936.72, 3288.74 cm^{-1}, deepithelialized goat skin (DS) at 1238.34, 1530.57, 1658.84, 2953.12, 3289.70 cm^{-1} and decellularized goat skin (AS) at 1238.34, 1547.93, 1666.55, 2953.12, 3306.10 cm^{-1}.

in the 500–4000 cm^{-1} wave number spectral range with a spectral resolution of 2 cm^{-1} and 45 scans [18]. The FTIR bone spectrum can be roughly separated into two regions where the organic and inorganic components have distinct peaks (**Figure 5**). The peak at 931.65 cm^{-1} assigned to the ν_1 phosphate band [25–27] is due to the symmetric stretching vibration of the apatitic phosphate ion (PO_4^{3-}) of hydroxyapatite [27, 28]. The peak at 1032.92 cm^{-1} corresponds to the ν_3 phosphate band [29, 30] is due to the asymmetric stretching vibration of the PO_4^{3-} [27, 31]. The ν_3 phosphate peak at 1032.92 cm^{-1} is coming from the nonstoichiometric hydroxyapatite which may contain CO_3^{2-} or HPO_4^{2-} or both in the apatite [27, 31]. With age, the concentration of CO_3^{2-} increases during apatite maturation, the amount of labile HPO_4^{2-} decreases, keeping the Ca/(C + P) atomic ratio almost constant [32]. The peaks at 1235.45 cm^{-1}, 1530.51 cm^{-1} and 1671.37 cm^{-1} correspond to the amide group, and they originate from the collagen [27]. The peak at 1235.45 cm^{-1} corresponds to the amide III results from mixed C-N stretch and N-H in-plane bend with additional contributions from C-C_α stretch [29]. The peak at 1530.51 cm^{-1} corresponds to the amide II which arises from the combined effect of C-N stretch and N-H in-plane bending [27, 31]. The peak at 1671.37 cm^{-1} corresponds to the amide I is due to the stretching vibration of the peptide carbonyl group (-C=O) along the polypeptide backbone [27]. The peak at 2879.82 cm^{-1} is asymmetric CH_2 stretch and it arises from the organic component [27]. The peak at 2965.82 cm^{-1} corresponds to the symmetric CH_2 and asymmetric CH_3 stretch of the organic component [27]. The peak at 3079.46 cm^{-1} corresponds to the amide B is due to asymmetric stretching of the CH_2 stretching vibration and the absorption due to the CH_2 alkyl chain [27]. The weak intensity peak at 3281.99 cm^{-1} corresponds to the amide A band of collagen is due to N-H stretching vibrations when the N-H group of the peptide is involved in hydrogen bonds [27]. The broad peak at 3536.60 cm^{-1} is attributed to the presence of the OH^- group [27, 33]. The transmittance peaks indicated the presence of inorganic ν_1, ν_3 PO_4^{3-}, OH^- in addition to organic collagen amide A, amide B, amide I, amide II and amide III chemical functional groups in the bovine cortical bone (**Figure 5**).

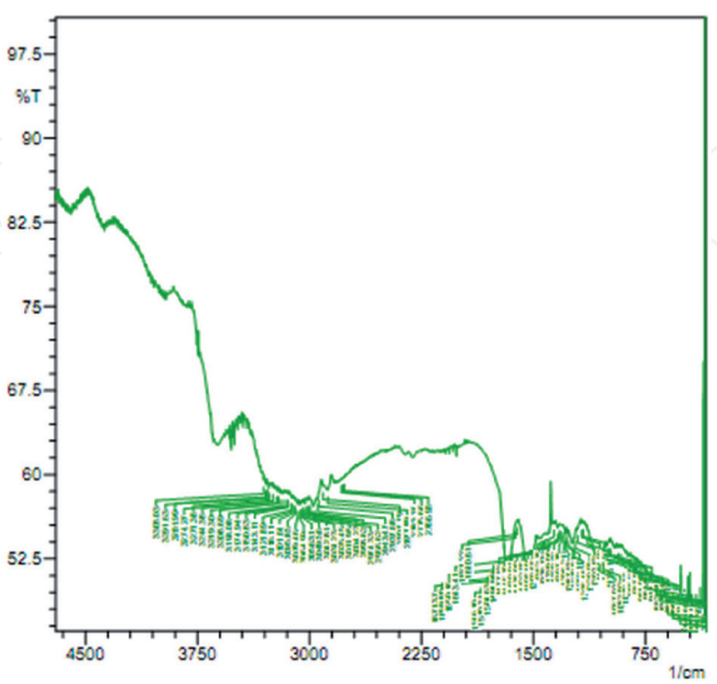

Figure 5.
FTIR spectrum of the native cortical bone showing transmittance peaks at 931.65, 1032.92, 1235.45, 1530.51, 1671.37, 2877.89, 2966.62, 3079.46, 3281.99, 3615 cm^{-1}.

4. Conclusions

The FTIR spectra of native and decellularized buffalo aortae, buffalo diaphragms, goat skin, and native bovine cortical bone are presented. The transmittance peaks are that of organic collagen amide A, amide B, amide I, amide II and amide III chemical functional groups in both native and decellularized aortae, diaphragms and skin. In bone, the transmittance peaks are that of inorganic CO_3^{2-}, ν_1, ν_3 PO_4^{3-}, OH^- in addition to organic collagen amide A, amide B, amide I, amide II and amide III chemical functional groups. These important transmittance peaks of the tissue samples will help researchers in defining the chemical structure of these animal tissues.

Author details

Vineet Kumar[1*], Shruti D. Vora[2], Foram A. Asodiya[2], Naveen Kumar[3] and Anil K. Gangwar[4]

1 Department of Veterinary Surgery and Radiology, College of Veterinary and Animal Sciences, Sardar Vallabhbhai Patel University of Agriculture and Technology, Meerut, Uttar Pradesh, India

2 Department of Veterinary Surgery and Radiology, College of Veterinary Science and Animal Husbandry, Junagadh Agricultural University, Junagadh, Gujarat, India

3 Division of Surgery, ICAR-Indian Veterinary Research Institute, Izatnagar, Uttar Pradesh, India

4 Department of Surgery, College of Veterinary Science and Animal Husbandry, Acharya Narendra Deva University of Agriculture and Technology, Ayodhya, Uttar Pradesh, India

*Address all correspondence to: bharadwaj374@gmail.com

References

[1] Kumar, V, Devarathnam, J, Gangwar, A. K, Kumar, N, Sharma, A. K, Pawde, A. M, & Singh, H. Use of acellular aortic matrix for reconstruction of abdominal hernias in buffaloes. Veterinary Record (2012)., 170, 392.

[2] Kumar, V, Kumar, N, Mathew, D. D, Gangwar, A. K, Saxena, A. C, & Remya, V. Repair of abdominal wall hernias using acellular dermal matrix in goats. Journal of Applied Animal Research (2013)., 41(1):117-120.

[3] Kumar, V, Gangwar, A. K, Mathew, D. D, Ahmad, R. A, Saxena, A. C, & Kumar, N. Acellular dermal matrix for surgical repair of ventral hernia in horses. Journal of Equine Veterinary Science (2013)., 33, 238-243.

[4] Kumar, V, Kumar, N, Gangwar, A. K, & Saxena, A. C. Using acellular aortic matrix to repair umbilical hernias of calves. Australian Veterinary Journal (2013)., 91, 251-253.

[5] Kumar, V, Kumar, N, Singh, H, Mathew, D. D, Singh, K, & Ahmad, R. A. An acellular aortic matrix of buffalo origin crosslinked with 1-ethyl-3-3-dimethylaminopropylcarbodiimide hydrochloride for the repair of inguinal hernia in horses. Equine Veterinary Education (2013)., 25, 398-402.

[6] Kumar, V, Kumar, N, Gangwar, A. K, & Singh H. Comparison of acellular small intestinal matrix (ASIM) and 1-ethyl-3-(3-dimethylaminopropyl) carbodiimide crosslinked ASIM (ASIM-EDC) for repair of full-thickness skin wounds in rabbits. Wound Medicine (2014)., 7, 24-33.

[7] Kumar, V, Kumar, N, Gangwar, A. K, Singh, H, & Singh, R. Comparative histological and immunological evaluation of 1,4-butanediol diglycidyl ether crosslinked versus noncrosslinked acellular swim bladder matrix for healing of full-thickness skin wounds in rabbits. Journal Surgical Research (2015)., 197, 436-446.

[8] Gangwar, A. K, Kumar, N, Devi, K. S, Kumar, V, & Singh R. Primary chicken embryo fibroblasts seeded 3-D acellular dermal matrix (3-D ADM) improve regeneration of full thickness skin wounds in rats. Tissue & Cell (2015)., 47, 311-322.

[9] Kumar, V, Gangwar, A. K, Kumar, N, & Singh, H. Use of the bubaline acellular diaphragm matrix for umbilical hernioplasty in pigs. Veterinarski Arhiv (2015)., 85, 49-58.

[10] Kumar, V, Gangwar, A. K, & Kumar, N. Evaluation of the murine dermal matrix as a biological mesh in dogs. Proceedings of the National Academy of Sciences, India Section B: Biological Sciences (2016)., 86, 953-960.

[11] Vora, S. D, Kumar, V, Asodiya, F. A, Singh, V. K, Fefar, D. T, & Gajera, H. P. Bubaline diaphragm matrix: development and clinical assessment into cattle abdominal hernia repair. Brazilian Archives of Biology & Technology (2019)., 62, e19180442.

[12] Kumar, V, & Vora, S. D. Abdominal wall repair with bubaline aortic matrix in a goat. Indian Journal of Small Ruminants (2019)., 25, 255-256.

[13] Asodiya, F. A, Kumar, V, Vora, S. D, Singh, V. K, Fefar, D. T, & Gajera, H. P. Preparation, characterization, and xenotransplantation of the caprine acellular dermal matrix. Xenotransplantation (2020)., 27, e12572.

[14] Vora, S. D, Kumar, V, Singh, V. K, Fefar, D. T, & Gajera, H. P. Bubaline aortic matrix: Histologic, imaging, Fourier transform infrared

spectroscopic characterization and application into cattle abdominal hernia repair. Proceedings of the National Academy of Sciences, India Section B: Biological Sciences (2020)., 90, 161-170.

[15] Kumar, V. Abdominal intercostal hernia in a cat (*Felis domestica*). Topics in Companion Animal Medicine (2020)., 40, 100437.

[16] Gilbert, T. W, Sellaroa, T. L, & Badylak, S. F. Decellularization of tissues and organs. Biomaterials (2006)., 27, 3675-3683.

[17] Kular, J. K, Basu, S, & Sharma, R. I. The extracellular matrix: Structure, composition, age-related differences, tools for analysis and applications for tissue engineering. Journal of Tissue Engineering (2014)., 5, 1.

[18] Kumar, V, Asodiya, F. A, Singh, V. K, & Gajera, H. P. Microscopic and spectroscopic characterization of an extraskeletal intranasal osteoma in a Gir cow. Microscopy Research & Technique (2020)., 00, 1-8 http://dx.doi.org/10.1002/jemt.23613.

[19] Devarathnam, J, Sharma, A. K, Kumar, N, & Rai, R. B. Optimization of protocols for decellularization of buffalo aorta. Journal of Biomaterials and Tissue Engineering (2014)., 4, 778-785.

[20] Doyle, B. B, Bendit, E, & Blout, E. R. Infrared spectroscopy of collagen and collagen-like polypeptides. Biopolymers (1975)., 14, 937-957.

[21] Abe, Y, & Krimm, S. Normal vibrations of crystalline polyglycine II. Biopolymers (1972)., 11, 1817-1839.

[22] Payne, K. J, & Veis, A. Fourier transform IR spectroscopy of collagen and gelatin solutions: Deconvolution of the Amide I band for conformational studies. Biopolymers (1988)., 387, 1949-1960.

[23] Krimm, S, & Bandekar, J. Vibrational spectroscopy and conformation of peptides, polypeptides, and proteins. Advances in Protein Chemistry (1986)., 38, 181-364.

[24] Muyonga, J. H, Cole, C. G. B, & Duodu, K. G. Characterisation of acid soluble collagen from skins of young and adult Nile perch (*Lates niloticus*). Food Chemistry (2004)., 85, 81-89.

[25] Rey, C, Shimizu, M, Collins, B, & Glimcher, M. Resolution-enhanced Fourier transform infrared spectroscopy study of the environment of phosphate ion in the early deposits of a solid phase of calcium phosphate in bone and enamel and their evolution with age: 2. Investigations in the $v3$ PO_4 domain. *Calcified Tissue International* (1991)., 49, 383-388.

[26] Thompson, T. J. U, Gauthier, M, & Islam, M. The application of a new method of Fourier transform infrared spectroscopy to the analysis of burned bone. Journal of Archaeological Science (2009)., 36, 910-914.

[27] Legan, L, Leskovar, T, Cresnar, M, Cavalli, F, Innocenti, D, & Ropret, P. Non-invasive reflection FTIR characterization of archaeological burnt bones: reference database and case studies. Journal of Cultural Heritage (2020)., 41, 13-26.

[28] Paschalis, E. P, DiCarlo, E, Betts, F, Sherman, P, Mendelsohn, R, & Boskey, A. L. FTIR microspectroscopic analysis of human osteonal bone. *Calcified Tissue International* (1996)., 59, 480-487.

[29] Rey, C, Renugopalakrishnan, V, Collins, B, & Glimcher, M. J. Fourier transform infrared spectroscopic study of the carbonate ions in bone mineral during aging. *Calcified Tissue International* (1991)., 349, 251-258.

[30] Wopenka, B, & Pasteris, J. D. A mineralogical perspective on the apatite in bone. Materials Science and Engineering: C (2005)., 25, 131-143.

[31] Paschalis, E. P, Betts, F, DiCarlo, E, Mendelsohn, R, & Boskey, A. L. FTIR microspectroscopic analysis of normal human cortical and trabecular bone. *Calcified Tissue International* (1997)., 61, 480-486.

[32] Combes, C, Cazalbou, S, & Rey, C. Apatite biominerals. Minerals (2016)., 6, 34.

[33] Akindoyo, J. O, Beg, M. D. H, Ghazali, S, & Islam, M. R. Effects of poly (dimethyl siloxane) on the water absorption and natural degradation of poly (lactic acid)/oil-palm empty-fruit-bunch fiber biocomposites. Journal of Applied Polymer Science (2015)., 132, 42784.